Co-Designed mm-Wave and LTE Handset Antennas

Joni Kurvinen, Henri Kähkönen, Anu Lehtovuori, Juha Ala-Laurinaho, and Ville Viikari, *Senior Member, IEEE*

***Abstract*— Fifth generation (5G) mobile networks will introduce several new frequencies for short-range high-capacity communications. Future handsets must also support current frequency bands for backward compatibility and long-range communications. This paper presents a proof-of-concept solution for co-designed millimeter-wave (mm-wave) and Long Term Evolution (LTE) antennas in a metal-rimmed handset. The design shows that both antenna types can be accommodated in a shared volume and be integrated into the same structure. Presented antennas operate at 700–960 MHz, 1710–2690 MHz, and 25–30 GHz. Simulations and measurements suggest that the system can be designed in such a way that the mm-wave antenna does not hinder the low-band performance. LTE antennas generally reach over 60% total efficiency while the mm-wave module has a peak gain of 7 dBi with measurement-verified beam-steering capability. The proposed design proves that 5G mm-wave antennas can be embedded to 4G systems without greatly sacrificing display size or sub-6 GHz antenna performance.**

***Index Terms*— Beam-steering, endfire, fifth generation (5G), handset antenna, Long Term Evolution (LTE), metal rim, millimeter-wave (mm-wave), Vivaldi antenna.**

I. Introduction

FIFTH GENERATION (5G) mobile networks will provide means for high-capacity communications by allocating new frequency bands in the RF-spectrum. The foreseen millimeter-wave (mm-wave) frequencies are expected to enable up to 1000 times higher data rates due to obtainable wide bandwidths [1]. Hence, the coming standard has raised interest to place mm-wave antennas in mobile devices, especially in the promising 28 GHz region, as shown in many recently published papers [2]–[12]. Besides the scientific community, also the industry is very interested in the available spectrum around 28 GHz [13]–[15].

Traditional ways to increase transmission rates include applying multiple-input multiple-output (MIMO) and carrier aggregation (CA) techniques. These methods require several antennas, and as known, the usable space for antennas in the mobile devices is very limited. Restricted volume is even more of a challenge for the Long Term Evolution (LTE) antennas, due to antennas required for other applications such as Wi-Fi and GPS. An increased number of antennas means reducing the size of a single antenna, which decreases its efficiency and weakens the overall performance. Especially at the LTE low band (LB) below 1 GHz, at which the antennas consume the most space, this challenge is emphasized. Furthermore, the LB antenna performance is easily deteriorated by other nearby antennas, even if they operate on different frequencies.

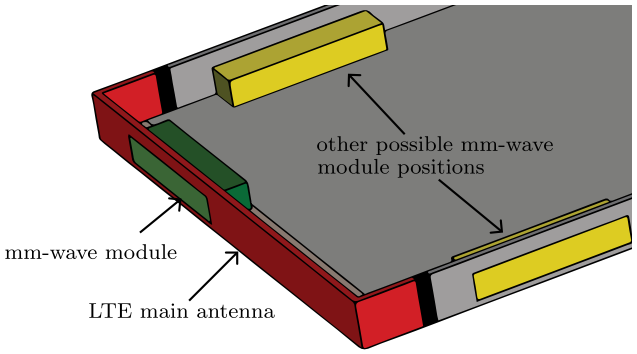

Fig. 1. Illustration of mm-wave antenna within the same volume with the LTE antenna. Other possible mm-wave module locations are marked with yellow.

As the space is limited, it is important to integrate the antennas into the body of the handset. At present, many commercial smartphones have a metal rim, which is commonly utilized for the LTE antennas [16]–[20]. However, the coming mm-wave antennas require beam-steering, and hence, the antenna is an array of small elements. Therefore, it is not practical to integrate them into the metal frame in the same way as LTE antennas. The whole mm-wave module requires space, and thus, it might negatively affect the sub-6 GHz antennas. For that reason, both antenna types should be considered while designing antennas for 5G smartphones.

To the best of authors' knowledge, there are not many papers that include both the LTE and the mm-wave antennas. This paper presents a proof-of-concept solution for the co-design of LTE and mm-wave antennas in the shared structure, in particular, in such a way that the same volume is required as when designing the LTE antennas only and still keeping the antennas well isolated and their performance not affected by each other. Fig. 1 illustrates the concept of embedding the mm-wave module in the LTE structure. Generally, similar mm-wave modules could be placed on all sides of the device for better coverage and connectivity, but in this paper, we focus on having the two antenna types within the same volume.

Traditionally, the short edges of a smartphone are reserved for the LTE main and diversity antennas. For example, in [3] and [12], mm-wave antennas are located on the sides

Manuscript received May 18, 2018; revised November 7, 2018; accepted December 8, 2018. Date of publication December 25, 2018; date of current version March 5, 2019. This work was supported by Business Finland, Nokia Bell Labs, Huawei Technologies Finland, RF360, Pulse Electronics Finland, and Sasken Finland through the 5G TRx Project. The work of J. Kurvinen was supported in part by the Aalto ELEC Doctoral School and in part by the Finnish Foundation for Technology Promotion. *(Corresponding author: Joni Kurvinen.)*

The authors are with the Department of Electronics and Nanoengineering, Aalto University School of Electrical Engineering, 00076 Espoo, Finland (e-mail: joni.kurvinen@aalto.fi).

Color versions of one or more of the figures in this paper are available online at http://ieeexplore.ieee.org.

Digital Object Identifier 10.1109/TAP.2018.2888823

of the phone due to this reason. In [4] and [6]–[9], the mm-wave antennas are located in the ends of the phone, but the LTE antennas, however, are not taken into account. In [2], both antenna types are considered, but the lowest supported LTE frequency is 1870 MHz. The proposed design in this paper is the first one to operate at both LTE LB and high band (HB) at 700–960 MHz and 1710–2690 MHz, respectively, besides the mm-wave band at 25–30 GHz.

Placing mm-wave antenna to the short edge of the device, as opposed to [3] and [12], enables simple MIMO implementation and is possibly less sensitive for user effect caused by hands. The mm-wave antenna can also be realized with low-cost printed circuit board (PCB) technology, unlike many others [3]–[5]. In addition, embedding the mm-wave antenna in the same module with the LTE antennas keeps the system compact and makes it easier to design the rest of the phone. Despite the shared volume, generally the two antennas can be designed separately as their radiation patterns and operational principles are different, and hence, the coupling between the antennas is minimal.

Nevertheless, introducing an mm-wave antenna to the same volume sets new restrictions for LTE antenna design. As we reserve certain areas for the mm-wave module, at the same time, we restrict for example feed positions for the LTE antenna. Also, mm-wave antenna requires modifications to be made to the metal rim, i.e., cut a plastic-filled window for the endfire radiation of the antenna. We demonstrate this with the LTE LB and HB antennas, but the same technique could also be applied for combining mm-wave antenna with other sub-6 GHz frequencies in the 5G spectrum as well as with 5 GHz Wi-Fi.

In this paper, we present the design of the mm-wave antenna embedded to the LTE antenna that could be implemented in a modern smartphone. One design goal of this co-design is that the mm-wave and LTE antennas would not interact and could, therefore, be designed separately, which greatly simplifies the design process. A prototype is built of this proof-of-concept system, and its performance is verified by measurements, including the beam-steering capability of the mm-wave antenna. The design compares well to other published antennas of the same frequency range and hence is promising for future smartphone use.

In Section II, we describe the design process and our goals in more detail. Section III presents the designed mobile Vivaldi antenna structure for the mm-wave communications. The co-design of the LTE system and the importance of the required plastic-filled window are presented in Section IV. Simulation and measurement results are shown and analyzed in Section V. Finally, conclusions are given in Section VI.

II. Design Process

The phone is modeled and antenna structures are designed and simulated in an electromagnetic 3-D simulator software CST Microwave Studio. For matching circuit design, we have used Optenni Lab.

The design process can be described with three main steps. First, we have designed the mm-wave antenna separately. After having that antenna working in the simulations, we moved to the LTE antennas. The space reservation for the mm-wave antenna is considered while designing the LTE antennas. Also, in this phase, we use the whole phone model, whereas in the initial mm-wave antenna design, we used only a small section of the metal frame. The final step is the co-design by embedding the mm-wave module to the LTE antenna. At this point, some fine-tuning of the dimensions and redesigning of matching circuit was required to achieve the desired performance. To verify the simulation results of the embedded antennas, we built and measured a prototype of the co-design.

A. Specifications

As we are presenting a proof of concept of a 5G handset antenna system, we use a simplified phone model with size of $150 \times 75 \times 7$ mm^3, which corresponds to the size of current popular commercial smartphones. Antennas are specified to operate at LTE frequencies 700–960 MHz and 1710–2690 MHz and at mm-wave frequency band 25–30 GHz.

The model that we use in our design is for common metal-rimmed phones. The LTE antennas are integrated to the side rim for efficient use of small available volume. The main PCB acts as an RF-ground for the antennas. The used substrate is 0.8-mm thick FR-4 ($\varepsilon_r = 4.3, \tan\delta = 0.025$), and copper plating models the display of the phone. The ground clearance for the LTE antennas is 10 mm.

The mm-wave antenna is implemented on a separate PCB, a 0.101-mm thick Rogers RO4350B substrate ($\varepsilon_r = 3.48, \tan\delta = 0.0037$) enclosed by PREPERM L450 ($\varepsilon_r = 4.5, \tan\delta = 0.0005$) RF-optimized injection moldable plastic. For appropriate radiation performance of the mm-wave antenna, a window must be cut into the metal rim. The size of the mm-wave block should be less than $25 \times 10 \times 6$ mm^3 in order to fit within the volume of the LTE antenna and to keep the window size reasonable.

B. Objectives

The performance of both antennas is evaluated with impedance matching, total efficiency, and also with the beam-steering capability in the mm-wave case. For the LTE antennas, the targets for the impedance matching and total efficiency are -6 dB and 60%, respectively, over the whole bands. In addition, the isolation should be at least 15 dB between LB and HB.

The impedance matching target for the mm-wave antenna is below -10 dB. Also, more than 6 dBi of realized gain is desired with ability to steer the beam at least $\pm 25°$.

The main objective is to show that we can achieve good individual performance in both the LTE and the mm-wave antennas in a co-designed system, where the antennas are placed within the same volume. Hence, it is critical that the two antennas do not deteriorate each other's performance. The aimed low interaction between the two antenna systems should enable us to design them separately, which significantly simplifies and speeds up the design process. As the focus is in the co-design, e.g., implementing MIMO capability to this

system is out of the scope of this paper. However, MIMO support is possible to include in the proposed solution in the future. Also, the large angular coverage of mm-wave antennas is not an interest in this paper. Only one module is studied while good coverage obviously requires more mm-wave antennas, as is illustrated in Fig. 1.

C. Challenges

Including the design of the mm-wave antennas in the handset design introduces new challenges. Compared to the LTE antennas, the main issue to take into account is the radiation pattern of the antenna. In typical use, the orientation of the handset is random, and hence, the connection to the base station must be ensured. LTE antennas have more or less omnidirectional patterns for this purpose, but the same solution cannot be applied to mm-wave antennas. This is due to the increased free-space loss. In our case, the difference in propagation losses is more than 20 dB between the LTE HB and mm-wave band.

To compensate the increased path loss, mm-wave antennas are used in arrays to produce narrow beam and thereby have more gain. However, narrow beam requires pointing directly toward the base station. Thus, mm-wave antennas have to be beam-steerable to handle the random handset orientation and unknown location of the base station.

Another difference is targeted matching levels. Whereas the LTE antennas are traditionally designed for matching level of -6 dB, mm-wave antennas are designed with target of at least -10 dB. Also, dual-polarization is desired by the industry from 5G antennas to avoid polarization mismatch losses and, hence, to improve the connectivity and link quality. However, realizing dual-polarized mm-wave antennas is out of the scope of this paper.

Having a system that supports low frequencies and over 10 times higher mm-wave band brings up simulation challenges. Simulating the whole band is computationally heavy and mostly unnecessary, thus, simulations are conducted separately for LTE and mm-wave bands. Another issue is that mm-wave structure consists of much smaller details due to the significantly shorter wavelength. Especially when simulating LTE bands this causes problems when constructing the mesh around the structure. Small details to be modeled properly in lower frequencies require a huge amount of mesh cells, which increases the simulation time remarkably. Last simulation challenges come up with the circuit simulations. The lumped elements that we are using for the LTE antennas are specified for up to 8 GHz only, and hence, we cannot by simulations investigate if the LTE antennas cause troubles in the mm-wave band.

III. mm-Wave Antenna

Tapered slot antennas or Vivaldi antennas are known to be good candidates for wideband beam-steerable antennas and their structure has been studied experimentally in linear and planar configurations [6], [21]. A single Vivaldi antenna is usually more than a wavelength in length and width but with such large elements would be difficult to fit inside a mobile phone and could not be electronically steered. In an array configuration, the mutual coupling between the antenna elements improves the matching compared to a similar isolated antenna. Typically, the mutual coupling is used in the optimization of larger electronically scanned arrays but the same method can also be applied successfully to smaller arrays when the elements are properly designed.

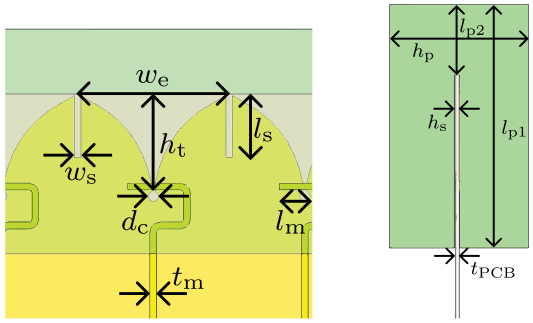

Fig. 2. Detailed figure of the Vivaldi element in the mm-wave antenna module from (a) top and (b) side. All dimensions are listed in Table I.

Here, a conventional Vivaldi antenna design with microstrip to slot-line transition is used in a linear four-element array. The structure is optimized to minimize the necessary volume inside the phone while still maintaining efficient radiation through the slot in the metal frame of the mobile phone. A larger array of, e.g., eight elements would produce higher gain but also consume more space inside the phone, which complicates the final co-design with the LTE antenna and placement in the short edge. Therefore, the long edges of the phone might be more feasible locations for larger arrays. The same design method, however, can be used to realize larger arrays too.

The antenna array is enclosed inside a plastic, which is used to cover the aperture that allows the antenna to radiate through the metal rim. In addition to filling the aperture, the plastic decreases the effective wavelength of the propagating field and thus enhances the radiation through the small hole. As a side effect, the antenna elements themselves can also be made slightly smaller to decrease the volume occupied by the whole module. Material properties play a large role in defining the dimensions for the antenna element and the aperture besides the matching of the antenna. Therefore, it is crucial to select materials with proper dielectric constant and low losses. The matching of the Vivaldi antenna in an array generally depends on the dimensions of the antenna elements and the spacing between them. Additional factors for the matching in this case are caused by the plastic-to-air interface and the size of the aperture in relation to the wavelength of the propagating field.

The Vivaldi antenna element structure is presented in Fig. 2 and the dimensions marked in the illustrations are explained in Table I. The tapering of the slot is defined as follows [21]:

$$x = c_1 e^{Ry} + c_2 \tag{1}$$

where

$$c_1 = \frac{x_2 - x_1}{e^{Ry_2} - e^{Ry_1}} \tag{2}$$

$$c_2 = \frac{x_1 e^{Ry_2} - x_2 e^{Ry_1}}{e^{Ry_2} - e^{Ry_1}} \tag{3}$$

TABLE I
DIMENSIONS OF THE VIVALDI ANTENNA

Symbol	Meaning	Value (mm)
d_c	cavity diameter	0.32
h_t	height of the tapering	3.05
w_e	element width	4.75
l_s	tuning slot length	2
w_s	tuning slot width	0.2
t_m	microstrip thickness	0.21
l_m	microstrip extension over the feed slot	0.8
l_{p1}	length of the plastic	7
l_{p2}	length of the plastic after the PCB	2
h_p	height of the plastic	4
h_s	slot height	0.15
t_{PCB}	PCB thickness	0.101

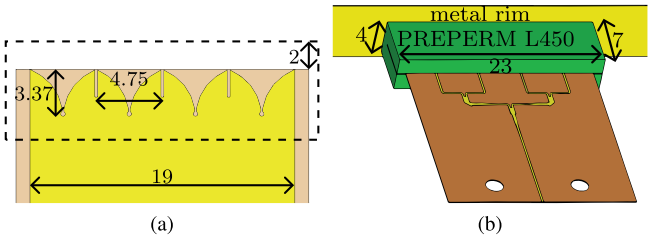

Fig. 3. (a) Structure of the mobile Vivaldi antenna. (b) Vivaldi structure is enclosed with PREPERM L450 plastic. All dimensions are in millimeters.

where y_1 and x_1 define the starting point of the tapering, and y_2 and x_2 define the endpoint. R is the opening rate of the tapered slot and it is used as an optimization parameter. The tapering slot is terminated to a circular cavity and the slot is fed with a microstrip which is terminated with a stub. Small cutouts are used between the elements to modify the mutual coupling between the elements to improve the matching. The used PCB substrate is 0.101-mm thick RO4350B as it provides reasonably good rigidity and low losses even with such a thin substrate. The plastic used to enclose the antenna array is PREPERM L450 with a dielectric constant of approximately 4.5. The selected dielectric offers a good compromise between the matching and the size of the hole in the metal rim. Higher permittivity of the plastic would slightly scale down the dimensions of the window but is, however, impractical to use as matching the antenna becomes a very challenging task. Fig. 3 shows the full antenna array and the plastic enclosure.

Ideally, each of the array elements would be fed with separate RF-chains or phase shifters to enable the electronic scanning. In this initial demonstration, however, three different PCBs with different progressive phase shifts between the elements are used. This enables us to measure three separate cases, which are used to demonstrate the beam-steering capability. In addition to the broadside radiation pattern, setups with 50° and 100° phase shifts between the elements were selected to be manufactured and measured. The different designs with the power dividers are shown in Fig. 4.

The size of the PCB for this demonstration is quite large and would not be used as such in a mobile phone. In an actual mobile phone with phase shifters or separate RF-chains, the antenna structure itself would only be approximately the size of the plastic used to enclose the PCB containing the antennas.

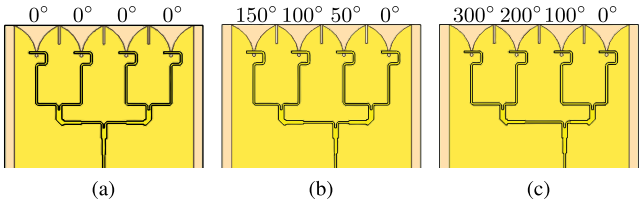

Fig. 4. Feed network with implemented phase-shifting structures. The progressive phase shift between the elements is (a) 0°, (b) 50°, or (c) 100°.

IV. CO-DESIGN OF THE LTE ANTENNA

The main objective of this co-design is to achieve good individual performance for both antennas. Crucial issue is to have the interaction between the two systems as low as possible.

A. Antenna Structure

The designed LTE antenna is integrated into the metal rim. The rim acts as a capacitive coupling element (CCE). It covers LTE LB at 700–960 MHz and HB at 1710–2690 MHz. Both bands are covered with the same element to save space for other possible antennas and subsystems in the device.

The antenna is placed at the lower end of the phone, which is the common location for the LTE main antenna. This configuration leaves the other end free for the diversity antenna for possible MIMO communications. However, the MIMO implementation is not included in this paper.

A CCE is chosen as the antenna type due to its simple and compact design and ability to achieve relatively wide bandwidth. Also, CCEs are commonly used in metal-rimmed smartphones [16], [22], [23], thus, it is a good choice for this proof-of-concept design. The structural optimization is done without the mm-wave module present, only its space reservation is taken into account, e.g., when choosing feed positions. In the optimization process, the matching circuitry plays a larger role than structural dimensions. When the mm-wave module is added to the design, the clearance and impedance of the LTE antenna change. Thus, the original matching networks become inapplicable and the circuitries must be redesigned.

LB and HB are realized with their own feeding structures to improve performance in both bands. Antenna structures and feeding networks are adopted from [20] and [24]–[26] combined with aperture matching. The structure is illustrated in Fig. 5. Due to the USB-port, the mm-wave module cannot be placed in the center of the rim and, thus, is located next to the USB. The module reserves nearly the whole area on its side, thus, LB and HB feeds are located on the opposite side. This also minimizes the possible negative effects of having the mm-wave module in the same volume with the LTE antennas. Fig. 6 shows the rim with the plastic-filled window that has aperture size of 23×4 mm^2.

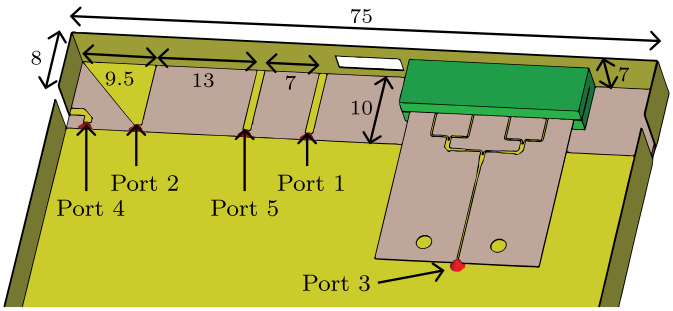

Fig. 5. Structure of the co-designed antennas. The mm-wave antenna is integrated to the same volume as the LTE antenna. All dimensions are in millimeters.

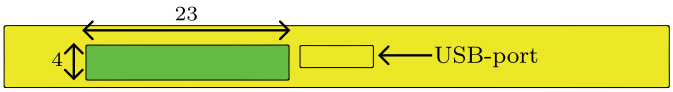

Fig. 6. Plastic-filled window in the metal rim for the mm-wave antenna. All dimensions are in millimeters.

Although the mm-wave antenna is embedded in the LTE antennas, the design still relies on traditional practices: 1) LB utilizes the maximum volume [23], [25]; 2) LB feed is in the center of the structure and aperture matching close to it [27]; and 3) HB feed is implemented in the corner of the ground plane [28] and supported with a triangular feeding strip [24]. The embedded design consumes roughly the same total volume as similar LTE solutions [20], [26], although less than 10 mm clearance have become a trend in recent publications [29]–[31]. By using a simple LTE structure with larger clearance, we can do a reliable study on the mm-wave antenna interaction.

The port numbers in Fig. 5 indicate the corresponding ports used in the simulations and when the performance results are presented later in Section V. Ports 1–3 refer to LB, HB, and mm-wave feeds, respectively. Ports 4 and 5 are used for aperture matching of the LTE bands. Aperture matching increases bandwidth and improves efficiency. In addition, the fixed passive structure is beneficial as it allows the use of carrier aggregation, unlike tunable structures. Matching circuits of the final design with used capacitor and inductor values are shown in Fig. 7. Lumped components are selected from Murata's LQW18 and GQM18 series, and their corresponding models are used in simulations.

B. Plastic-Filled Window

The plastic-filled window is the key difference between this design and other metal rim antennas from the LTE point-of-view. The window itself is required for the radiation of the mm-wave element, as a solid metal frame would block the mm-wave radiation from exiting the structure. The plastic filling is needed for the visual aspects and sealing of a smartphone besides its effect on the antenna matching. Removing the plastic would significantly alter the matching levels of the antenna and, hence, shift the resonance frequency to be out of the desired band resulting in strong sidelobes and weakened realized gain. As the Vivaldi array is optimized to this plastic-filled window, we obtain a similar radiation pattern and efficiency as a normal Vivaldi array in the free space without any mobile phone structures surrounding it.

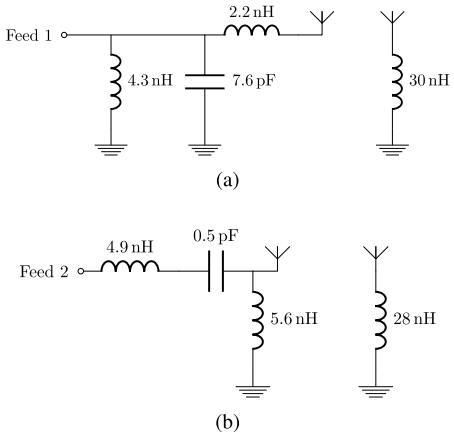

Fig. 7. Matching circuits and aperture matching components used in (a) Ports 1 and 5 for LB and (b) Ports 2 and 4 for HB.

The size of the window is optimized to be as small as possible but still large enough for the mm-wave module. The height of the window should be at least half of the effective wavelength, which favors for filling the window with high-permittivity material to keep the window practically small. Otherwise, the propagating wave is below cutoff and will not radiate. On the other hand, the LTE element requires a path for currents, and therefore, the rim cannot be completely cut to separate pieces. The width of the window is determined by the number of elements in the Vivaldi array. Increasing the number elements in the array, e.g., to improve gain and scanning angle would make the plastic-filled window larger. Thus, the LTE antenna should be redesigned to avoid overlapping the mm-wave module with the LTE feeds.

The main source of interaction between the mm-wave and LTE antennas is the plastic-filled window. In practice, the mm-wave antenna is only affected by the window in the metal rim, and as far as the window dimensions are known, the LTE antenna does not need to be taken into account in the design of the mm-wave antenna. However, the LTE antenna is sensitive to the mm-wave module as it affects the clearance and impedance of the LTE antenna. The effect, however, is small enough so that the LTE antenna shape does not need to be redesigned but only the matching network.

Windows in the metal rim could act as slot antennas. This clearly is not desired as the designed antennas are CCEs and a Vivaldi array. Fig. 8 shows the simulated surface currents at all operational bands. At the LTE bands, in Fig. 8(a) and (b), the current is distributed evenly in the rim, and thus, the effect of the slot on the radiation is small. Especially at the mm-waveband, it is clear that the Vivaldi array produces the radiation. Moreover, working beam-steering capability requires the radiating element to be the antenna array instead of the window.

V. Prototype Experiments

The prototype is manufactured carefully based on the simulation model according to the specifications described in

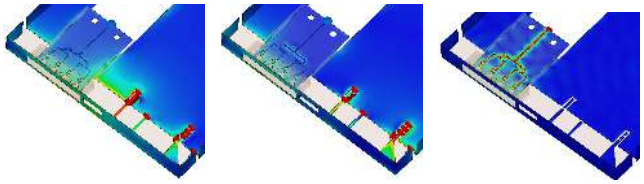

(a) (b) (c)

Fig. 8. Surface currents at (a) 800 MHz, (b) 2.4 GHz, and (c) 28 GHz.

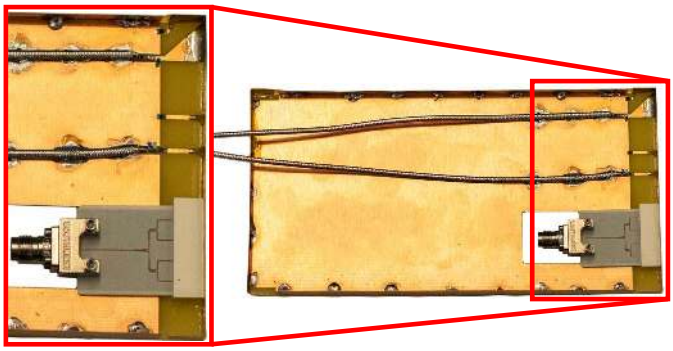

Fig. 9. Manufactured prototype.

Section II-A. The prototype is shown in Fig. 9. The metal frame is made of 0.125-mm thick laser-cut tin-bronze alloy. The plastic enclosing the mm-wave PCB is glued to the chassis. The main PCB is modified with a milled hole to fit the end-launch connector required for mm-wave feeding. Before manufacturing the prototype, it was verified by simulations that the hole in the ground plane does not affect the LTE performance.

A. Measurement Setups

The measurements consisted of *S*-parameter measurements with vector network analyzer and far-field measurements. The far-field of the LTE antenna was measured with MVG StarLab and mm-wave antenna with NSI2000 planar near-field scanner equipped with WR-28 measurement probe. Both measurement systems measure the near-field of the antenna, and then perform a near-field-to-far-field transformation.

B. mm-Wave Performance

Matching levels for the three different beam-steering angles are shown in Fig. 10. In each case, the simulated and the measured reflection coefficients behave differently. Despite the differences between simulations and measurements, the antenna is very well matched with at least −10 dB across the whole band for all three phase shifters.

Another important factor for the mm-wave antenna is the beam-steering capability. Fig. 11 shows this performance at 26 and 28 GHz. In Fig. 11(a), we notice that measurements match with simulations rather well at 26 GHz and the desired beam-steering directions are obtained, the maximum direction locating around ±30°. Peak realized gains are around 5–7 dBi in measurements. Simulated values are slightly higher with 50° or 100° progressive phase shifts.

Fig. 11(b) shows that the realized gain patterns are similar in simulations and measurements at 28 GHz. However, the measured peak values are around 5 dBi, which is 2 dB less than

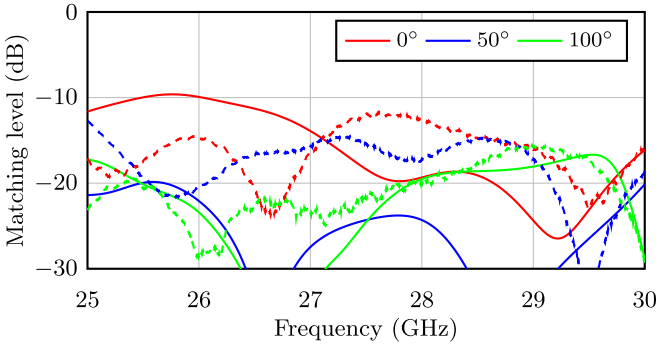

Fig. 10. Input matching of the Vivaldi antenna for three implemented phase shifters. Solid lines: simulations. Dashed lines: measurements.

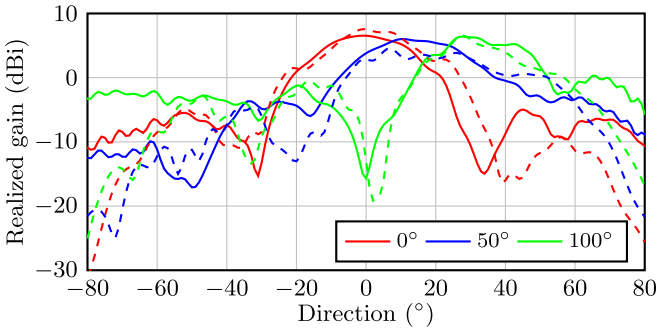

(a)

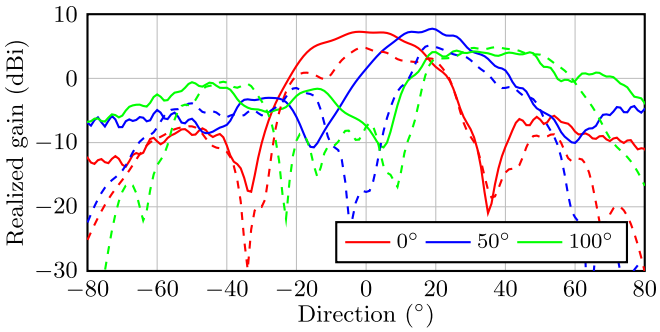

(b)

Fig. 11. Azimuth plane realized gain patterns of the mobile Vivaldi antenna array at (a) 26 GHz and (b) 28 GHz. Solid lines: simulated patterns. Dashed lines: measured patterns.

in simulations, except in 100° case, which is of same level. The desired beam-steering directions are also achieved at this frequency, with the maximum at almost ±40°.

The differences between simulations and measurements might be caused by inaccuracies in the manufacturing process. Possible reasons are that the PCB is not pushed deep enough inside the plastic, the PCB is not centered and aligned with the plastic, or the whole module is slightly tilted with respect to the chassis and the window in the frame. Both steps of assembling the mm-wave prototype, i.e., attaching the PCB to the narrow drilling in the plastic and placing the module into the chassis, are done manually by hand. At mm-wave frequencies, the tolerances are very tight, and even misalignments of fractions of a millimeter will affect the antenna performance. However, this structure is quite robust against these small errors, as its measured performance is very good despite the differences to simulations, especially in matching.

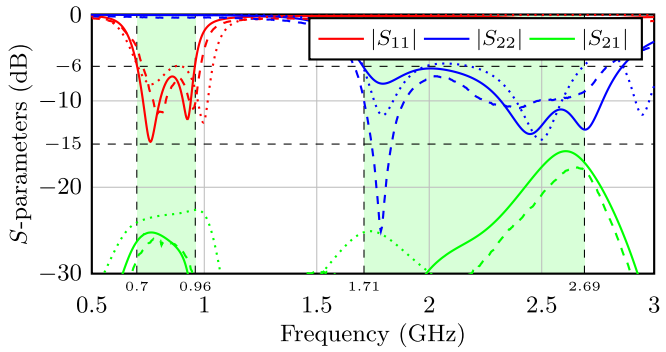

Fig. 12. *S*-parameters of the LTE antenna in the co-design. Solid lines: simulations. Dashed lines: measurements. Dotted lines: simulated *S*-parameters without the mm-wave module with the original matching circuits.

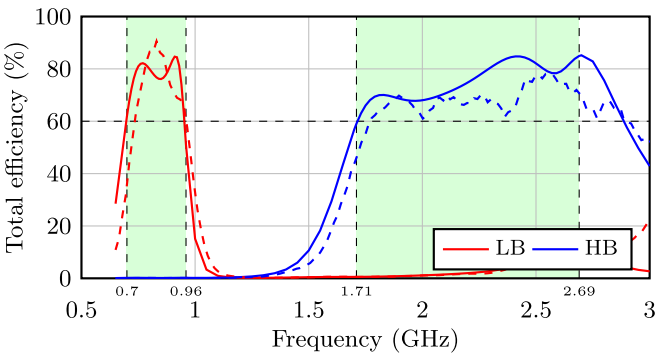

Fig. 13. Total efficiency of the LTE antenna in the co-design. Solid lines: simulations. Dashed lines: measurements.

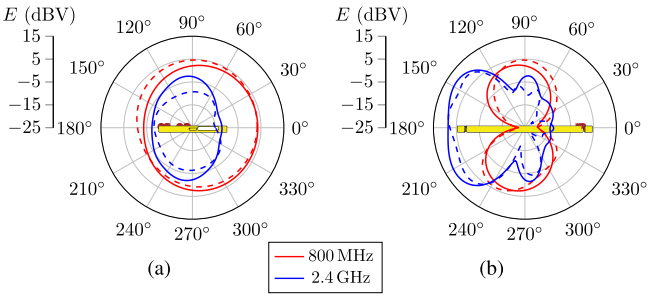

Fig. 14. Total *E*-field patterns of the LTE antenna at 800 MHz and 2.4 GHz in (a) azimuth and (b) elevation planes at a reference distance of 1 m. Solid lines: simulated radiation patterns. Dashed lines: measured patterns. Front face of the phone is toward 270° in both cuts.

As the exact mm-wave frequency bands are not yet allocated, the used band varies remarkably in different publications. In [6], [10], and [12], the supported band is just around 28 GHz, while our antenna and designs in [3], [4], [7]–[9], and [11] are able to operate on a several gigahertz-wide band around 28 GHz. Peak gain varies mainly from 5 to 15 dBi between publications, whereas our maximum realized gain is 7 dBi. However, our array consists of only four elements, while all other designs have eight or even more elements. Smaller array also allows the module to be physically more compact. In particular, we have verified the beam-steering capability by measurements, while other works have only simulated that. Even though the coverage is better in broadside patterns, the verified beam-steering significantly improves our endfire array. Also, our module is easily applicable to different MIMO configurations for better coverage. Considering the small array size of our mobile Vivaldi design, it performs very well against other published mm-wave antennas for smartphones.

C. LTE Performance

The measured and simulated *S*-parameters are shown in Fig. 12. The system achieves −6 dB impedance matching for both bands, and despite realizing LB and HB in the same element the mutual coupling between them is below −15 dB. The measured *S*-parameters agree with simulations well as matching on both bands is also at least −6 dB and coupling is slightly better than in simulations. The figure also shows that the effect of adding the mm-wave module to the LTE structure is small enough as the matching levels are good after redesigning the matching networks. Coupling between LTE and mm-wave antennas is below −40 dB in the operational LTE bands in simulations. In addition, in a realistic system, both antenna types would have their own RF-transceivers. As the operational bands are far from each other, the direct port-to-port coupling between the systems would not be an issue in this case.

The total antenna efficiency is over 60% for both bands in simulations, as Fig. 13 presents. In measurements, a similar performance is achieved. At the LB, the measured efficiency is 50% at band edges but peaks at 90%, i.e., higher than in simulations. At HB, the measured efficiency varies between 60% and 80% with slightly lower maximum values than in simulations.

Fig. 14 shows the total *E*-field radiation patterns at both LTE bands in the azimuth and elevation planes. As desired, the azimuth patterns are pretty omnidirectional, and hence, the predicted pattern is not heavily affected by the mm-wave module. The measured patterns are pretty similar with simulations. Small differences between the simulated and measured patterns are most likely caused by the end-launch connector attached to the mm-wave PCB, which was not included in the simulations. For example, at 2.4 GHz, the total efficiency is good but in the azimuth plane the radiation pattern level is clearly lower in measured results than in simulated ones. Also, it is noticed that the antennas radiate better toward other directions, as in elevation plane the simulated and measured patterns are almost identical.

Comparing the LTE performance of this design with similar previously proposed antennas [17], [19], [20] shows our performance is of the same level in total efficiency. The main difference is that in many of other publications the lowest supported frequency is around 800 MHz [19], [20]. In [17], the whole LB is supported, but its reconfigurable structure allows only to use very narrow frequency bands at a time. Our passive implementation covers the whole band and supports carrier aggregation.

D. State-of-the-Art Comparison

To the best of authors' knowledge, a combined LTE and mm-wave smartphone antenna systems have been published only in [2], which therefore can be considered as the

TABLE II
COMPARISON OF THIS PAPER WITH THE STATE-OF-THE-ART

FoM	**This work**	[2]
LTE		
Volume (one antenna)	**75 x 8 x 7 mm^3**	9 x 30 x 0.965 mm^3
Low band	**700–960 MHz**	None
High band	**1710–2690 MHz**	1870–2530 MHz
Efficiency	**50–90 %**	50–83 %
MIMO	**No**	Yes
mm-Wave		
Volume	**23 x 7 x 4 mm^3**	23.2 x 8.3 x 0.965 mm^3
Band	**25–30 GHz**	26–28.4 GHz
Pattern	**Endfire**	Broadside
Peak realized gain	**7 dBi**	8.2 dBi
Array size	**1 x 4**	2 x 4
Beam-steering	**$\pm$25°**	Not verified

current state-of-the-art. Despite the design goals having been different, the compared figures-of-merit (FoM) are collected in Table II.

In LTE operations, our design outperforms [2] with larger supported bands and slightly higher peak efficiencies. Although our design does not have MIMO support, it could simply be implemented to the other end of our device. Moreover, [2] covers only a small LTE band with rather large antenna element, thus with MIMO support the space consumption is significant.

In mm-wave performance, our design covers significantly larger frequency spectrum in the possible 5G band around 28 GHz. Also, the proposed system achieves nearly the same peak realized gain with smaller array. The design in [2] probably covers a larger area with its broadside radiation pattern compared to our endfire radiation but to improve our coverage we have verified by measurements a working beam-steering capability. Also, our mm-wave module can be placed within the same volume that the LTE antenna consumes, whereas [2] requires additional space.

This paper excludes many realistic and probably required aspects of future smartphones. Continuation work includes, e.g., realizing dual-polarization and larger beam-steering coverage at the mm-wave band and implementing MIMO at LTE bands. As the plastic-enclosure of the mm-wave antenna allows a low interaction with the LTE antenna, it is likely that the same co-design method could be used with other mm-wave structures as well. Then, e.g., a dual-polarized array could be included in this structure. In this design, we demonstrated the beam-steering capability with only three cases but with real phase shifters, we can have larger phase shifts between the elements and, thus, wider beam-steering coverage. Also, the general angular coverage can be simply improved by adding more similar mm-wave modules around the phone, as we suggested in Fig. 1. Furthermore, the gain of the array could be enhanced by increasing the number of elements as far as there is space available to increase the physical dimensions of the mm-wave antenna.

VI. CONCLUSION

This paper presented a proof-of-concept co-design for mm-wave and LTE antennas in a shared volume inside a metal-rimmed handset. Measurement results show that both antennas can operate independently without deteriorating each other's performance. Implementing both LTE LB and HB on the same structure saves space, and the used multifeed system enables good performance with total efficiency being over 60%. The Vivaldi array designed for mm-wave communications enables wideband performance around 28 GHz with measured peak realized a gain of 7 dBi. The structure also supports beam-steering angles of at least $\pm$25°, which is verified by measurements with three different power division feed networks. Designing the mm-wave and LTE antennas separately allowed us to achieve good individual performance, as the interaction between the two systems remained small. The presented design demonstrates a promising way of realizing LTE and mm-wave antennas on the same volume for future handsets.

ACKNOWLEDGMENT

The authors would like to thank E. Kahra for his help in manufacturing the prototypes.

REFERENCES

[1] J. G. Andrews *et al.*, "What will 5G be?" *IEEE J. Sel. Areas Commun.*, vol. 32, no. 6, pp. 1065–1082, Jun. 2014.

[2] R. Hussain, A. T. Alreshaid, S. K. Podilchak, and M. S. Sharawi, "Compact 4G MIMO antenna integrated with a 5G array for current and future mobile handsets," *IET Microw., Antennas Propag.*, vol. 11, no. 2, pp. 271–279, Jan. 2017.

[3] B. Yu, K. Yang, C.-Y.-D. Sim, and G. Yang, "A novel 28 GHz beam steering array for 5G mobile device with metallic casing application," *IEEE Trans. Antennas Propag.*, vol. 66, no. 1, pp. 462–466, Jan. 2018.

[4] M. Stanley, Y. Huang, T. Loh, Q. Xu, H. Wang, and H. Zhou, "A high gain steerable millimeter-wave antenna array for 5G smartphone applications," in *Proc. 11th Eur. Conf. Antennas Propag. (EuCAP)*, Paris, France, Mar. 2017, pp. 1311–1314.

[5] W. Hong, K. Baek, Y. Lee, and Y. G. Kim, "Design and analysis of a low-profile 28 GHz beam steering antenna solution for future 5G cellular applications," in *IEEE MTT-S Int. Microw. Symp. Dig. (IMS)*, Tampa, FL, USA, Jun. 2014, pp. 1–4.

[6] N. Ojaroudiparchin, M. Shen, and G. F. Pedersen, "Design of Vivaldi antenna array with end-fire beam steering function for 5G mobile terminals," in *Proc. 23rd Telecommun. Forum (TELFOR)*, Belgrade, Serbia, Nov. 2015, pp. 587–590.

[7] N. Ojaroudiparchin, M. Shen, and G. F. Pedersen, "End-fire phased array 5G antenna design using leaf-shaped bow-tie elements for 28/38 GHz MIMO applications," in *Proc. IEEE Int. Conf. Ubiquitous Wireless Broadband (ICUWB)*, Nanjing, China, Oct. 2016, pp. 1–4.

[8] M. Stanley, Y. Huang, A. Alieldin, and S. Joseph, "A novel mm-Wave phased array antenna for 180° coverage for 5G smartphone applications," in *Proc. 12th Eur. Conf. Antennas Propag. (EuCAP)*, London, U.K., Apr. 2018, pp. 1–3. [Online]. Available: https://ieeexplore.ieee.org/document/8568480

[9] S. Zhang, I. Syrytsin, and G. F. Pedersen, "Substrate-insensitive phased array with improved circularly-polarized scan angle for 5G mobile terminals," in *Proc. 12th Eur. Conf. Antennas Propag. (EuCAP)*, London, U.K., Apr. 2018, pp. 1–5.

[10] A. Tatomirescu, A. Oprian, S. Zhekov, and G. F. Pedersen, "Beam-steering array for handheld devices targeting 5G," in *Proc. Int. Symp. Antennas Propag. (ISAP)*, Hobart, TAS, Australia, Nov. 2015, pp. 1–4.

[11] S. Zhang, X. Chen, I. Syrytsin, and G. F. Pedersen, "A planar switchable 3-D-coverage phased array antenna and its user effects for 28-GHz mobile terminal applications," *IEEE Trans. Antennas Propag.*, vol. 65, no. 12, pp. 6413–6421, Dec. 2017.

[12] R. Rodríguez-Cano, S. Zhang, and G. F. Pedersen, "Beam-steerable multi-band mm-wave bow-tie antenna array for mobile terminals," in *Proc. 12th Eur. Conf. Antennas Propag. (EuCAP)*, London, U.K., Apr. 2018, pp. 1–4.

[13] "The 5G mmWave revolution," Nokia, Espoo, Finland, White Paper SR1610000323EN, 2016. [Online]. Available: https://onestore.nokia.com/asset/200779
[14] "5G systems," Ericsson, Stockholm, Sweden, White Paper UEN 284 23-3251, 2017. [Online]. Available: https://www.ericsson.com/assets/local/publications/white-papers/wp-5g-systems.pdf
[15] *5G Spectrum Public Policy Position*, Huawei, Shenzhen, China. 2018
[16] J. Kurvinen, A. Lehtovuori, J. Mai, C. Wang, and V. Viikari, "Metal-covered handset with LTE MIMO, Wi-Fi MIMO, and GPS antennas," *Prog. Electromagn. Res. C*, vol. 80, pp. 89–101, 2018. [Online]. Available: http://www.jpier.org/PIERC/pier.php?paper=17082303
[17] M. Stanley, Y. Huang, H. Wang, H. Zhou, Z. Tian, and Q. Xu, "A novel reconfigurable metal rim integrated open slot antenna for octa-band smartphone applications," *IEEE Trans. Antennas Propag.*, vol. 65, no. 7, pp. 3352–3363, Jul. 2017.
[18] C.-K. Chang, W.-J. Liao, and C.-C. Tsai, "Metal body-integrated open-end slot-antenna designs for handset LTE uses," *IEEE Trans. Antennas Propag.*, vol. 64, no. 12, pp. 5436–5440, Dec. 2016.
[19] Y.-L. Ban, Y.-F. Qiang, Z. Chen, K. Kang, and J.-H. Guo, "A dual-loop antenna design for hepta-band WWAN/LTE metal-rimmed smartphone applications," *IEEE Trans. Antennas Propag.*, vol. 63, no. 1, pp. 48–58, Jan. 2015.
[20] D. Lee, W. C. Choi, J. Ahn, and Y. J. Yoon, "A simple monopole antenna for hepta-band LTE/WWAN metal-framed mobile phone," in *Proc. Int. Symp. Antennas Propag. (ISAP)*, Hobart, TAS, Australia, Nov. 2015, pp. 1–3.
[21] J. Shin and D. H. Schaubert, "A parameter study of stripline-fed Vivaldi notch-antenna arrays," *IEEE Trans. Antennas Propag.*, vol. 47, no. 5, pp. 879–886, May 1999.
[22] K. Rasilainen, A. Lehtovuori, A. Boussada, and V. Viikari, "Carrier aggregation compatible MIMO antenna for LTE handset," *Prog. Electromagn. Res. C*, vol. 78, pp. 1–10, 2017. [Online]. Available: http://www.jpier.org/PIERC/pier.php?paper=17061204
[23] R. Valkonen, M. Kaltiokallio, and C. Icheln, "Capacitive coupling element antennas for multi-standard mobile handsets," *IEEE Trans. Antennas Propag.*, vol. 61, no. 5, pp. 2783–2791, May 2013.
[24] J. Ilvonen, R. Valkonen, J. Holopainen, and V. Viikari, "Design strategy for 4G handset antennas and a multiband hybrid antenna," *IEEE Trans. Antennas Propag.*, vol. 62, no. 4, pp. 1918–1927, Apr. 2014.
[25] R. Valkonen, J. Ilvonen, C. Icheln, and P. Vainikainen, "Inherently non-resonant multi-band mobile terminal antenna," *Electron. Lett.*, vol. 49, no. 1, pp. 11–13, Jan. 2013.
[26] H. Chen and A. Zhao, "LTE antenna design for mobile phone with metal frame," *IEEE Antennas Wireless Propag. Lett.*, vol. 15, pp. 1462–1465, 2016.
[27] A. Lehtovuori, J. Ilvonen, K. Rasilainen, and V. Viikari, "Single-element handset antenna design for modern smartphones: An industrial approach," in *Proc. 11th Eur. Conf. Antennas Propag. (EuCAP)*, Paris, France, Mar. 2017, pp. 2960–2963.
[28] A. Lehtovuori, R. Valkonen, and J. Ilvonen, "Designing capacitive coupling element antennas with bandwidth estimators," *IEEE Antennas Wireless Propag. Lett.*, vol. 13, pp. 959–962, 2014.
[29] Y. Liu, Y. Luo, and S. Gong, "An antenna with a stair-like ground branch for octa-band narrow-frame mobile phone," *IEEE Antennas Wireless Propag. Lett.*, vol. 17, no. 8, pp. 1542–1546, Aug. 2018.
[30] Y.-L. Ban, Y.-F. Qiang, G. Wu, H. Wang, and K.-L. Wong, "Reconfigurable narrow-frame antenna for LTE/WWAN metal-rimmed smartphone applications," *IET Microw. Antennas Propag.*, vol. 10, no. 10, pp. 1092–1100, Apr. 2016.
[31] J.-W. Lian, Y.-L. Ban, Y.-L. Yang, L.-W. Zhang, C.-Y.-D. Sim, and K. Kang, "Hybrid multi-mode narrow-frame antenna for WWAN/LTE metal-rimmed smartphone applications," *IEEE Access*, vol. 4, pp. 3991–3998, 2016.

Joni Kurvinen was born in Espoo, Finland, in 1991. He received the B.Sc. (Tech.) and M.Sc. (Tech.) (with distinction) degrees in electrical engineering from Aalto University, Espoo, in 2014 and 2016, respectively, where he is currently pursuing the D.Sc. (Tech.) degree.

Since 2016, he has been a Research Assistant with the Department of Electronics and Nanoengineering, School of Electrical Engineering, Aalto University. His current research interests include handset antennas in 5G and MIMO systems.

Henri Kähkönen was born in Lohja, Finland, in 1989. He received the B.Sc. (Tech.) and M.Sc. (Tech.) degrees in electrical engineering from Aalto University, Espoo, Finland, in 2015 and 2017, respectively, where he is currently pursuing the D.Sc. (Tech.) degree.

Since 2016, he has been a Research Assistant with the Department of Electronics and Nanoengineering, School of Electrical Engineering, Aalto University. His current research interests include wideband, beam-steerable antenna arrays, especially at millimeter-wave spectrum.

Anu Lehtovuori received the M.Sc. (Tech.) and Lic.Sc. (Tech.) degrees in electrical engineering from the Helsinki University of Technology, Espoo, Finland, in 2000 and 2003, respectively, and the D.Sc. (Tech.) degree in electrical engineering from Aalto University, Espoo, in 2015.

She is currently a University Lecturer in circuit theory with the School of Electrical Engineering, Aalto University. Her current research interests include electrically small antennas and design of antennas for mobile devices.

Juha Ala-Laurinaho received the Diploma Engineer (M.Sc.) degree in mathematics and the D.Sc. (Tech.) degree in electrical engineering from the Helsinki University of Technology (TKK), Espoo, Finland, in 1995 and 2001, respectively.

He has been with the Radio Laboratory, TKK, from 1995 to 2007, with the Department of Radio Science and Engineering from 2008 to 2016, and currently with the Department of Electronics and Nanoengineering, School of Electrical Engineering, Aalto Univeristy. In 1995, he was a Research Assistant, and since 1996, he has been a Research Associate, and currently, he is a Staff Scientist. He has also been a Project Manager in many millimeter-wave technology related projects. His current research interests include antennas and antenna measurement techniques for millimeter and submillimeter waves and the millimeter-wave imaging.

Ville Viikari (S'06–09–M'09–SM'10) was born in Espoo, Finland, in 1979. He received the M.Sc. (Tech.) and D.Sc. (Tech.) (with distinction) degrees in electrical engineering from the Helsinki University of Technology (TKK), Espoo, in 2004 and 2007, respectively.

From 2001 to 2007, he was with the Radio Laboratory, TKK, where he was involved in antenna measurement techniques at submillimeter wavelengths and antenna pattern correction techniques. From 2007 to 2012, he was a Research Scientist and a Senior Scientist with the VTT Technical Research Centre, Espoo, where he was involved in wireless sensors, RFID, radar applications, MEMS, and microwave sensors. He is currently an Associate Professor and the Deputy Head of the Department with the School of Electrical Engineering, Aalto University, Espoo. His current research interests include antennas for mobile networks, RF-powered devices, and antenna measurement techniques.

Dr. Viikari has served as the Chair for the Technical Program Committee of the ESA Workshop on Millimeter-Wave Technology and Applications and the Global Symposium on Millimeter Waves in 2011 and 2016, in Espoo, Finland. He was a recipient of the Young Researcher Award of the Year 2014, presented by the Finnish Foundation for Technology Promotion, the IEEE Sensors Council 2010 Early Career Gold Award, the 2008 Young Scientist Award of the URSI XXXI Finnish Convention on Radio Science, Espoo, and the Best Student Paper Award of the Annual Symposium of the Antenna Measurement Techniques Association, Newport, RI, USA, in 2005.